RSC Advances

ROYAL SOCIETY OF CHEMISTRY

www.rsc.org/advances

Journal Name

ARTICLE

Angstrom-sized tungsten carbide promoted platinum electrocatalyst for effective oxygen reduction reaction and resource saving

Received 00th January 20xx,
Accepted 00th January 20xx

DOI: 10.1039/x0xx00000x

www.rsc.org/

Meng Xie[a], Meiping Zhang [b], Wei Wei[b], Zhifeng Jiang[b], Yuanguo Xu*[b]

Abstract: Angstrom-sized tungsten carbide dots (WC^{dot}), WC rods (WC^{rod}) and 10-nm-sized WC particles (WC^{nano}) are synthesized and used as platinum (Pt) electrocatalyst supports for efficient oxygen reduction reaction (ORR). The concentration of tungsten source and formula structure of carbon source (ion-exchange resin) control the size and shape of the WC materials. The angstrom-sized WC^{rod} promoted Pt electrocatalyst (Pt/WC^{rod}) shows slightly higher activity than the 10-nm-sized WC^{nano} promoted electrocatalyst (Pt/WC^{nano}), although the WC^{rod} costs only one tenth the W amount of the WC^{nano}, indicating resource saving. In addition, the Pt/WC^{rod} shows higher ORR efficiency and stabilization than the commercial Pt/C. The electron transfer from WC to Pt is believed to account for the excellent performances of the Pt/WC. The significances of the work are that less WC and less Pt can be used to achieve the same or higher ORR performances, and the synthesis method can also be used to synthesize other angstrom-sized materials.

Keywords: Angstrom-size; Tungsten carbide; Platinum electrocatalyst; Oxygen reduction reaction; Resource saving

1. Introduction

Oxygen electro-reduction reaction (ORR) has slow kinetics [1,2], which requires electrocatalyst with large loading of noble metal to increase the cathode current, thus causing high cost of low temperature fuel cells. Transition metal carbides can be used as catalyst promoters to promote activity and stability of the noble metal based electrocatalysts through synergistic effect [3-12] due to electron transfer from carbides to noble metals. The addition of carbides facilitates ORR and can reduce loading of noble metals to some extent [13-21].

Carbide particle size is a critical factor to determine its extent of promotion effect on noble metal electrocatalyst [22, 23]. It is thought that atomic level mixture of carbide and noble metal in electrocatalyst would lead to their full interactions. Precursors of both carbon and metal affect the metal carbide particle size. Traditional synthesis method through carburization of tungsten oxide (WO_3) leads to micro-sized tungsten carbide (WC) particles. Mixing carbon powder and ammonium metatungstate solution leads to 40-nm-sized WC particles [24]. Mixing solution of glucose (carbon source) and ammonium metatungstate leads to about 30-nm-sized WC particles [25, 26]. Mixing surfactant and tungsten precursor can further reduce WC particle size to about 15 nm [27, 28]. Ion-exchange resin as carbon source can reduce WC particle size to about 5 nm [29, 30]. To further reduce WC particle size to atomic level is a great challenge.

Herein, we report synthesis of WC materials with at least one-dimension of around 1 nm (angstrom-scale) through an ion-exchange method. Pt particles were then loaded on these WC materials and tested as electrocatalysts for ORR. Results show that the 1-nm-sized WC promoted electrocatalyst has higher activity than 10-nm-sized one, despite that the former only has one tenth the WC content of the latter. The ORR stability of the angstrom-sized WC promoted electrocatalyst is also excellent. This work indicates that nanometer-sized materials can be further reduced in size for higher activity and resource saving.

2. Experimental

2.1 Chemistry material

Polyacrylic weak-base anion-exchange resin (D201×1 resin, Hebi Power Resin Factory, China). Ammonium metatungstate (AMT, A.R., Tianjin Jinke Fine Chemicals, China). Chloroplatinic acid solution (H_2PtCl_6, A. R., Sinopharm Chemical Reagent Co., Ltd) and 20 ml glycol (A.R., Tianjin FuyuFine Chemicals Co., Ltd, China). Nafion (DuPont, USA). All chemicals were of analytical grade and used without further purification.

2.2 Synthesis of angstrom- and 10-nm-sized WC

A 10 g amount of polyacrylic weak-base anion-exchange resin was impregnated by 100 mL of 0.3 $mmol \cdot L^{-1}$ ammonium metatungstate (AMT) solution about 6 h, then separated, dried at 80

[a] School of Pharmacy, Jiangsu University, 301 Xuefu Road, Zhenjiang, 212013, P. R.China;
[b] School of Chemistry and Chemical Engineering, Jiangsu University, 301 Xuefu Road, Zhenjiang, 212013, P. R.China.
† * Corresponding author E-mail addresses: xuyg@ujs.edu.cn

℃ and calcined in N_2 atmosphere at 800 ℃ for 1 h. When the sample was cooled to room temperature, it was grinded to obtain the angstrom-sized WC material with rod shape (denoted as WC^{rod}).

Repeating the above process but change the AMT concentration to 3 or 0.06 mmol·L^{-1}, 10-nm-sized WC (denoted as WC^{nano}) and angstrom-sized WC with dot shape (denoted as WC^{dot}) were obtained.

2.3 Preparation of electrocatalysts

Typically, WC material (60 mg) was put into a mixture, which contained chloroplatinic acid solution (H_2PtCl_6, 5.33 ml, containing 40 mg Pt) and 20 ml glycol. Then, it was ultrasonicated for 30 min to obtain a well-dispersed ink. Its pH was then adjusted to 10 by 1 mol L^{-1}NaOH/glycol solution. The sample was then treated by a 900 W microwave oven for heating at a 10 s on and 10 s off process for 12 times [27,31]. After that, the resultant catalyst was washed and dried in vacuum at 40℃ for 24 h, and the Pt/WC electrocatalyst was obtained. The Pt particles supporting on WC^{nano}, WC^{rod} and WC^{dot} were denoted as Pt/WC^{nano}, Pt/WC^{rod} and Pt/WC^{dot}, respectively. The Pt contents in these electrocatalysts were 40 wt%. The accurate Pt contents were tested by inductively coupled plasma-atomic emission spectrometry (ICP, USA).

2.4 Synthesisof electrodes

Pt/WC (5 mg) and commercial Pt/C (4 mg, 47.6 wt% Pt, Japan) were dispersed in a solution containing 1.95 ml ethanol and 0.05 ml 5 wt% Nafion with the assistant of ultrasonic and got electrocatalyst ink, respectively. The ink (0.005 ml) was loaded on the surface of a glass carbon electrode (0.25 cm^2) and dried naturally. The total Pt content was 0.02 mg cm^{-2}.

2.5 Electrochemical characterization

The electrochemical properties of the samples were performed in an O_2-saturated 0.1 mol L^{-1} $HClO_4$ solution scanned between 0 to 1.1 V (vs. RHE) at a scan rate of 5 mV s^{-1}, 1600 rpm and kept at 25℃. A reversible hydrogen electrode (RHE) and a Pt foil (1.0 cm^2) were used as reference and counter electrodes, respectively.

2.6 Physical characterization

Transmission electron microscopy (TEM) micrographs were obtained with a JEOL-JEM-2010 (JEOL, Japan) operating at 200 kV. The crystal phase of the samples was analyzed by X-ray diffraction (XRD) analysis using an X-ray diffractometer (XRD, Japan, $Cu_{K\alpha}$, λ=1.54 Å) at a scan rate of 10° min^{-1} in the region (2θ) from 20° to 80°.

3. Results and discussion

WC^{nano}, WC^{rod} and WC^{dot} were prepared by a facile calcination method, and then Pt was introduced on their surface to form the electrocatalysts. The structure and shape of the catalyst were measured. The ORR properties and the stabilities of the samples were measured and the results showed that the Pt/WC has better performance than the Pt/C. The interaction between the Pt and the tungsten carbide is beneficial for the enhanced ORR ability.

Fig. 1 exhibits the XRD patterns of the WC^{nano}, WC^{rod} and WC^{dot}. The peaks at 31.5°, 35.6° and 48.3° ascribed to the (001), (100) and (101) crystal facets of WC. The peak intensities reduce with the decrease of AMT concentrations, which correspond to the reduction of WC contents and particle sizes. It is obvious that no other W compounds (oxides and W_2C) or W metal exist. Since WC is more efficient than the other W compounds or W metal in exerting promotion effect [32-35], this synthesis method of WC is highly efficient.

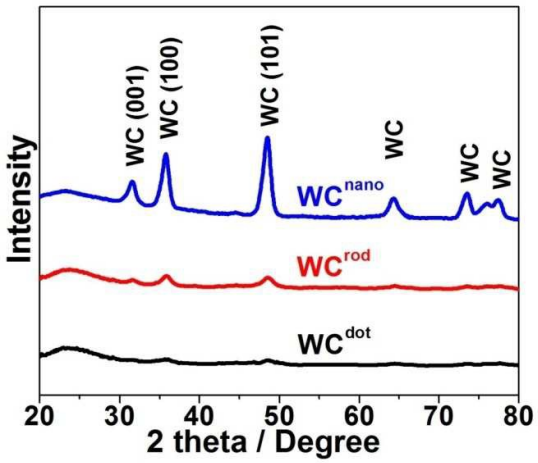

Fig. 1 XRD patterns of the WC^{nano}, WC^{rod} and WC^{dot}

Fig. 2a is the TEM image of the WC^{rod}, it can be seen that the width of WC rods is about 1 nm and the length is about several nanometers. The WC rods are well-dispersed in carbonized resin. Fig. 2b and its inset are HRTEM images of the WC^{rod}. It is clear that a rod with width of 1.7 nm, length of 6.0 nm and facet lattice of WC (100) can be observed. Fig. 2c shows the TEM image of the WC^{nano}, which shows WC particles with the diameters of around 10 nm. Fig. 2d is the TEM image of the WC^{dot}, the dots are too small to be clearly seen. The WC^{nano}, WC^{rod} and WC^{dot} were synthesized with different AMT concentrations; the above results indicate that the AMT concentration controls the shape and size of the WC materials.

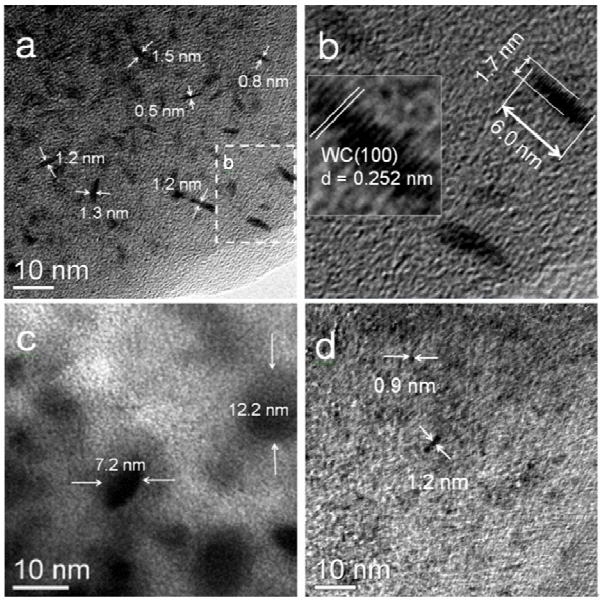

Fig. 2 (a) TEM and (b) HRTEM images of the WC^{rod}, (c) TEM image of the WC^{nano}, and (d) TEM image of the WC^{dot}. Inset of (a) is TEM image of WC^{rod} synthesized at 1100 °C for 2 h.

The structure of the ion-exchange resin (D201×1) and concentration of AMT (or ratio of resin to AMT) may also play roles on the sizes and shapes of WC particles. Fig. 3 shows the structural formula of the ion-exchange resin, which has long-chain. It can be seen that a high concentration of AMT results in agglomerated WC chain (WC^{nano}); a medium concentration of AMT results in discontinuous WC chain (WC^{rod}); and a low concentration of AMT results in dotted distribution of WC (WC^{dot}). The effect of heating temperature and time on morphology of WC was also studied. We changed the heating process to 1100 °C for 2 h and 550 °C for 1 h, and got WC^{rod} and WO_3^{rod} respectively. It is found that both the particles have the similar sizes and shapes to the WC^{rod} that is synthesized at 800 °C for 1 h (TEM images are not shown). The results indicate that the structure of resin and ratio of resin to AMT decide the size and shape of WC^{rod}.

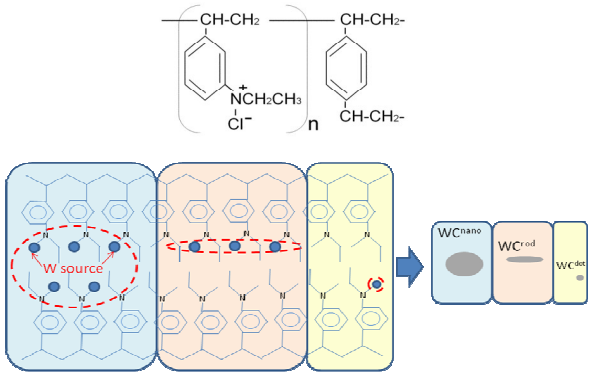

Fig. 3 The formula of D201×1 resin (n=2000) and effect of composition of resin and ratio of resin to AMT on the size and shape of WC

Pt/WC electrocatalysts were prepared by loading Pt particles on the as-synthesized WC materials. Fig. 4 shows XRD patterns of the Pt/WC^{nano}, Pt/WC^{rod} and Pt/WC^{dot} electrocatalysts. Except the peaks ascribed to WC, the peaks at 39.8°, 46.2° and 67.5° are ascribed to the (111), (200) and (220) crystal facets of Pt, respectively. It shows that the Pt peaks of Pt/WC^{rod} and Pt/WC^{dot} are wider than that of Pt/WC^{nano}, indicating that the Pt particles in Pt/WC^{rod} and Pt/WC^{dot} are smaller than those in Pt/WC^{nano}.

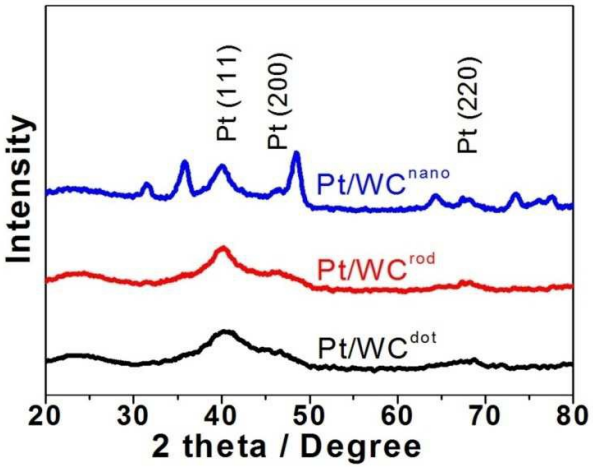

Fig. 4 XRD patterns of the Pt/WC^{nano}, Pt/WC^{rod} and Pt/WC^{dot}

Fig. 5 shows TEM images of the Pt/WC^{nano}, Pt/WC^{rod} and Pt/WC^{dot} electrocatalysts. Insets in Fig. 5a, 5c and 5d are the corresponding Pt particle size distributions that arerandomly selected (the numer of Pt particles is 100). Due to that these WC materials have different WC contents (leading to different densities or specific surface areas), Pt particles on these WC materials show different distributions and sizes. It can be seen that Pt distribution on WC^{rod} is moderate, on WC^{nano} is dense, and on WC^{dot} is sparse. The average Pt diameters are calculated as 2.3 nm on WC^{rod}, 3.4 nm on WC^{nano} and 2.4 nm on WC^{dot}, respectively. The results are matched with the XRD results (Fig. 4). Fig. 5b is the HRTEM image of the Pt/WC^{rod}, displaying the WC (100) and Pt (111) lattices. The inset EDS pattern of Fig. 5b confirms the existence of C, W and Pt elements (the existence of Cu and Cr element are ascribed to the bottom bush). The WC particles are very difficult to be discerned from Pt particles, since they are overlapped and have the similar sizes; moreover, the angstrom-sized WC has too low degree of crystallization to be identified from its crystal lattices. However, the Pt particles on WC-C composite should be as follows: Some Pt particles are on surface of WC, some are around WC and some are on surface of C [36]. In addition, Pt particles in commercial Pt/C are uniformly dispersed and the average Pt diameter is calculated to be 2.7 nm from its TEM image (not shown).

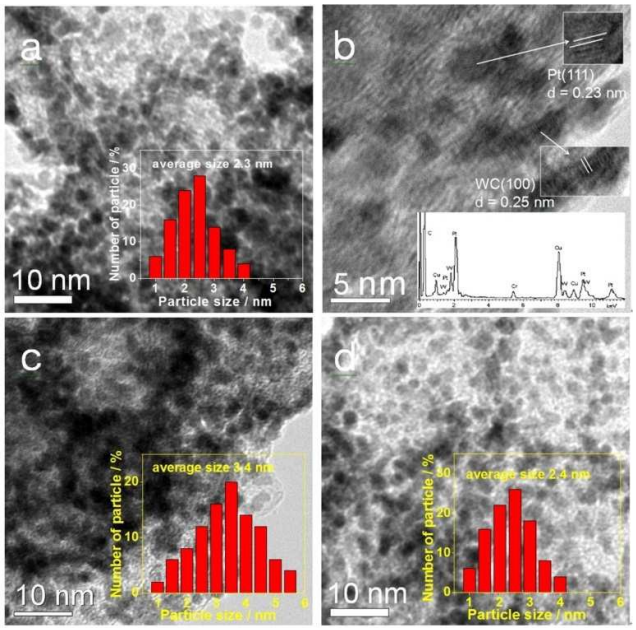

Fig. 5 (a) TEM and (b) HRTEM images of the Pt/WC^{rod}, (c) TEM image of the Pt/WC^{nano}, and (d) TEM image of the Pt/WC^{dot} Inset of (b) is the corresponding EDS pattern; insets of (a), (c) and (d) are the corresponding Pt particle size distributions

The ORR performances of the Pt/WC^{nano}, Pt/WC^{rod}, Pt/WC^{dot} and the commercial Pt/C electrodes were performed in 0.1 mol·L^{-1} $HClO_4$ solution (which is O_2-saturated) with the scan rate of 5 mV·s^{-1}, at 25℃, 1600 rpm (Fig. 6). Fig. 6a exhibits that the onset potentials of them are in the following sequence: Pt/WC^{rod} = Pt/WC^{nano} (+1.03 V) >Pt/WC^{dot} (+1.02V) >Pt/C (+1.01 V). The half-potential ($E_{1/2}$) values of them are in the following sequence: Pt/WC^{rod} (+0.888 V) >Pt/WC^{nano} (+0.880 V) >Pt/WC^{dot} (+0.861 V) >Pt/C (+0.849 V). Both the onset potentials and $E_{1/2}$ values of ORR on all the Pt/WC electrocatalysts are higher than those of the Pt/C, which suggests the doped WC significantly reduces ORR over potential.

Fig. 6b displays the kinetic currents of the electrocatalysts calculated from the experimental data by the mass transport correction for rotating disk electrode [37]:

$$i_k = i_d i/(i_d - i) \qquad (1)$$

where i is the experimentally resulted current, i_d is the tested diffusion-limited current and i_k is the mass-transport-free kinetic current. The mass activity (i_m) is determined from the calculation of i_k by equation (1), and which is normalized to the introduced Pt amount. The mass activities at +0.9 V for the electrocatalysts were investigated and the results were displayed in Table 1. It is clear that the mass activities of the electrocatalysts are in the following sequence: Pt/WC^{rod} (236.1 mA·mg$_{Pt}^{-1}$) >Pt/WC^{nano} (219.7 mA·mg$_{Pt}^{-1}$) >Pt/WC^{dot} (147.6 mA·mg$_{Pt}^{-1}$) >Pt/C (119.5 mA·mg$_{Pt}^{-1}$). The results indicate that the addition of WC greatly improves the ORR activity of Pt electrocatalysts. Therein, the mass activity of the typical Pt/WC^{rod} is 2.0 times of Pt/C. The ORR mass activities of the self-made Pt/WC^{rod} at 0.9 V or 0.85 V were also compared with other Pt/WC catalysts in literatures, as shown in Table 2. It can be seen that the Pt/WC^{rod} has the similar activity to Pt/WC (5 nm-sized WC), but much higher activity than the common WC (more than 5 nm in diameter) promoted Pt catalysts.

The inset of Fig. 6a displays the cyclic voltammograms (CV) of the electrocatalysts in N_2-saturated 0.1 mol·L^{-1} $HClO_4$solutionat 25 ℃ with the scan rate of 50 mV·s^{-1}. In all the CV curves, the peaks in the potential range of 0-0.25 V are come from the adsorption and desorption of hydrogen on the Pt surface. The peaks above 0.6 V in the anodic scan are due to oxidation of Pt, while peaks between 0.9 V and 0.5 V in the cathodic scan are due to reduction of PtO. The active surface areas (EASAs) of the electrocatalysts could be calculated by equation (2) [38]:

$$EASA = \frac{Q}{Q_H} = \frac{1}{Q_H}\left[\frac{1000}{a_0 v_0} \times \int_{E_1}^{E_2} (I - I_0) d(E - E_1)\right] \qquad (2)$$

Where E refers to the potential (V) and I refers to the measured current density (mA·cm^{-2}); I_0, E_1 and E_2 refer to the current density and potentials at the initial and terminal points of hydrogen desorption peak, which are marked in the Fig. 6a; a_o is the Pt loading normalized to the electrode surface area (mg$_{Pt}$·cm^{-2}), v_o is the scan rate (mV·s^{-1}), Q is the electric quantity in the hydrogen desorption peak and normalized to Pt loadings (C·g$_{Pt}^{-1}$), and Q_H the hydrogen adsorption electric quantity for a smooth polycrystalline Pt (Q_H =2.10 C·m^{-2})[27]. The calculated EASAs are also summarized in Table 1. They are in the following order: Pt/WC^{rod} (62.4 m^2·g$_{Pt}^{-1}$) >Pt/WC^{dot} (57.1 m^2·g$_{Pt}^{-1}$) >Pt/C (51.4 m^2·g$_{Pt}^{-1}$) >Pt/WC^{nano} (40.1 m^2·g$_{Pt}^{-1}$). The order is completely consistent with the Pt size order: Pt/WC^{rod} (2.3 nm) <Pt/WC^{dot} (2.4 nm) <Pt/C (2.7 nm) <Pt/WC^{nano} (3.4 nm). Both the Pt/WC^{rod} and Pt/WC^{dot} have higher EASAs than the Pt/WC^{nano}, which is due to the lower WC contents in both the WC^{rod} and WC^{dot}. As has been pointed out above, lower WC content means lower density or higher specific surface area, leading to uniform dispersion of Pt particles. However, the WC^{rod} has higher WC content than the WC^{dot}, but the EASA of Pt/WC^{rod} is a little higher than the Pt/WC^{dot}. The reason is that strong interaction existing between WC and Pt [3] benefits dispersion of Pt particles too. More WC content means more interaction with Pt, favouring the introduced Pt particles in smaller size to some extent. Therefore, to obtain higher EASA of Pt/WC electrocatalyst, the WC content should be moderate.

The values of the i_m/EASA(i_m normalized to the EASA) are also displayed in Table 1. It is clear that with the increase of WC contents (carbon powder <WC^{dot}<WC^{rod}<WC^{nano}), the values of i_m/EASA of the electrocatalysts increase (Pt/C <Pt/WC^{dot}<Pt/WC^{rod}<Pt/WC^{nano}), proving the promotion effect of WC on Pt. It is worth noting that although the WC^{nano} has higher promotion effect than WC^{rod}, the Pt/WC^{rod} has higher Pt mass activity than the Pt/WC^{nano}. The reason is that the Pt/WC^{rod} has more EASA than the Pt/WC^{nano} (Table 1). Therefore, the promotion effect from WC and the EASA from Pt

decide the ORR activity. Consequently, the WC content could be carefully adjusted to get higher Pt mass activity.

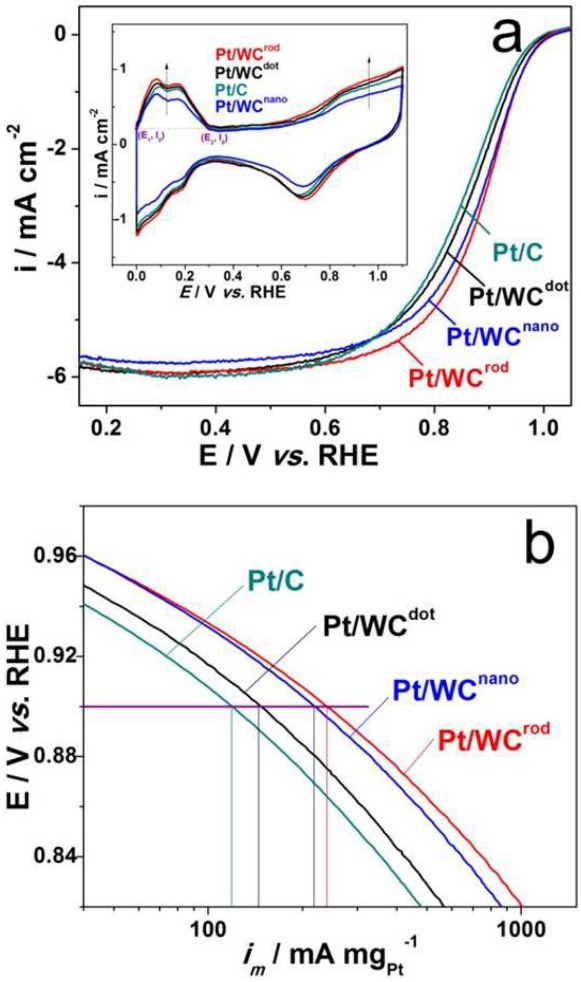

Fig. 6 (a) ORR curves of the electrodes at the initial cyclic voltammetry cycles in O_2-saturated 0.1 mol L^{-1} $HClO_4$ solution with the scan rate of 5 mV·s^{-1} at 25℃, 1600 rpm, (b) the corresponding mass activities of the electrocatalysts; inset of (a) is the cyclic voltammograms (CV) of the electrocatalysts in N_2-saturated 0.1 mol L^{-1} $HClO_4$ solution at 25℃ with the scan rate of 50 mV ·s^{-1}

In order to investigate the ORR stability of the typical Pt/WC^{rod} electrocatalyst, the 1st and 1000th ORR curves cycles of the Pt/WC^{rod} and Pt/C are tested in an O_2-saturated 0.1 mol·L^{-1} $HClO_4$ solution and the results are shown in Fig. 7. After the 1000 cycles, the corresponding $E_{1/2}$ values decreased 9 mV for Pt/WC^{rod} and 15 mV for Pt/C (Fig. 7a), respectively. The corresponding mass activities (Fig. 7b) at +0.9 V of them were computed by equation (1) and the results are displayed in Table 3. It can be seen that the Pt/WC^{rod} electrocatalyst has the activity retention of 90.4% while the Pt/C has only 77.6% after the 1000 cycles. The inset of Fig. 7a shows that the EASAs have the similar retentions as the ORR mass activities after the 1000 cycles. These findings indicate excellent electrocatalytic stability of the Pt/WC^{rod}.

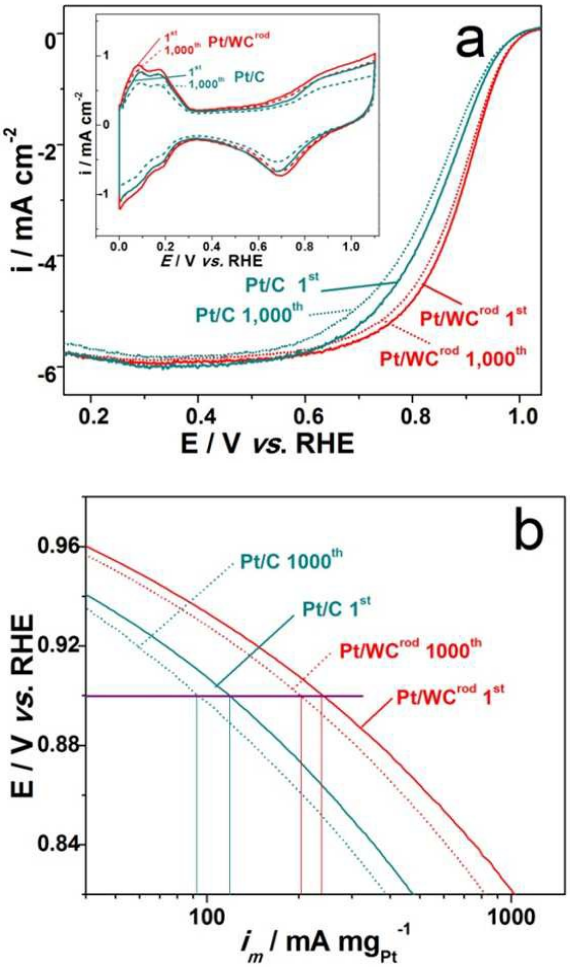

Fig. 7 (a) ORR curves of the Pt/WC^{rod} and Pt/C at the 1st and 1000th cycles in O_2-saturated 0.1 mol·L^{-1} $HClO_4$ solution with the scan rate of 5 mV·s^{-1} at 25℃, 1600 rpm, (b) the corresponding mass activities at the 1st and 1000th cycles; inset of (a) is the CV curves of the electrocatalysts in N_2-saturated 0.1 mol L^{-1} $HClO_4$ solution at 25℃ with the scan rate of 50 mV s^{-1} after the ORR curves of 1st and 1000th cycles

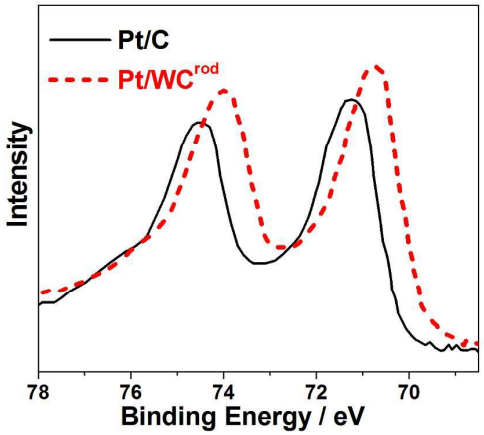

Fig. 8 XPS spectra of the Pt 4f on Pt/WC^{rod} and Pt/C

It is known that electrons can transfer between carbides and the loaded noble metals [3,38]. Fig. 8 shows XPS spectra of the Pt 4f on Pt/C and Pt/WC^{rod}. Obviously, negative shift occurred in XPS spectra after the introduction of WC^{rod}. The result indicates that there is electron-donating (transfer) from WC to Pt, which, on one hand, enhancing the ORR activity due to improved electron cloud density, and on the other hand, improves its stability due to the interaction force between WC and Pt.

Table 1 The EASAs and mass activity of the electrocatalysts

Electrocatalyst	Pt mass content*	i_m at 0.9 V (mA mg_{Pt}^{-1})	EASA (m^2 g_{Pt}^{-1})	i_m/EASA (mA m^{-2}_{Pt})
Pt/WC^{rod}	37.7%	236.1	62.4	3784
Pt/WC^{nano}	37.5%	219.7	40.1	5479
Pt/WC^{dot}	38.2%	147.6	57.1	2585
Pt/C	47.6%	119.5	51.4	2325

* The data were determined by inductively coupled plasma-atomic emission spectrometry (ICP)

Table 2 ORR activity comparison of the electrocatalysts

Electrocatalyst	i_m at 0.9 V (mA mg_{Pt}^{-1})	i_m at 0.85 V (mA mg_{Pt}^{-1})
Pt/WC^{rod} (self made)	236.1	620
Pt/WC (5 nm-sized WC) [36]	247.7	
Pt/WC (5-10 nm-sized WC) [14]	207.4	
Pt/WC [39]	too low	287
Pt/WC [13]	too low	181

Table 3 The ORR stability comparison of the Pt/WC^{rod} and Pt/C electrocatalysts

Electrocatalyst	CV cycle	i_m at 0.9 V (mA mg_{Pt}^{-1})	Activity retention
Pt/WC^{rod}	1st	236.1	90.4%
	1,000th	213.5	
Pt/C	1st	119.5	77.6%
	1,000th	92.7	

Conclusions

Angstrom-sized WC rods, WC dots and 10-nm-sized WC particles have been synthesized. The AMT concentration and formula structure of the ion-exchange resin control the size, shape and content of WC materials. The higher WC content leads to higher promotion effect on Pt electrocatalyst, but too high WC content results in large Pt particles due to reduced specific surface area. On the other hand, the lower WC content leads to smaller Pt particles, but too small WC content results in less promotion effect on Pt and slightly increased Pt sizes (or reduced EASAs) because of reduced interaction between WC and Pt. The WC^{rod} with moderate WC content leads to both considerable promotion effect on Pt and EASA of Pt electrocatalyst. The typical Pt/WC^{rod} shows higher Pt mass activity for ORR than the Pt/WC^{dot} (with less WC content), Pt/WC^{nano} (with more WC content) and Pt/C (without WC). The activity of Pt/WC^{rod} (236.1 mA·mg_{Pt}^{-1}) is 2.0 times that of commercial Pt/C (119.5 mA·mg_{Pt}^{-1}), indicating potential economic value. It is significant that the Pt/WC^{rod} shows slightly higher ORR activity than the Pt/WC^{nano}, but the WC^{rod} costs only one tenth of amount of W precursor of the WC^{nano} during the synthesis process, indicating resource saving. Although the cost saving from reduction of the WC may be negligible in the total cost of the catalyst, the method could be used to synthesize other angstrom-sized materials to reduce consumption and cost and benefit sustainable development of the world. Moreover, the Pt/WC^{rod} electrocatalyst possesses much higher ORR stability than commercial Pt/C. The efficient electron transfer between the two materials is believed to increase the electron cloud density of Pt and the linkage between WC and Pt, leading to enhanced ORR activity and stability of the Pt/WC electrocatalysts.

Acknowledgements

This work is financially supported by the National Natural Science Foundation of China for Youths (No. 21407065, 21506079), Natural Science Foundation of Jiangsu Province for Youths (BK20140533), China Postdoctoral Science Foundation (No.2014M551520, 2014M560399), Jiangsu Postdoctoral Science Foundation (1401143C) and Jiangsu University Scientific Research Funding (14JDG164).

Notes and references

1 J. Ge, J. St-Pierre and Y. Zhai, *Electrochim. Acta*, 2014, **134**, 272-280.
2 M. F. Li, L. W. Liao, D. F. Yuan, D. Mei and Y. X. Chen, *Electrochim. Acta*, 2013, **110**, 780-789.
3 G. Cui, P. K. Shen, H. Meng and J. Zhao and G. Wu, *J. Power Sources,* 2011, **196**, 6125-6130.
4 L. Wang, T. Du, J. Cheng, X. Xie, B. Yang and M. Li, *J. Power Sources,* 2015, **280**, 550-554.
5 Z. X. Yan, M. M. Zhang, J. M. Xie, J. J. Zhu and P. K. Shen, *Appl. Catal. B,* 2015, **165**, 636-641.
6 L. Elbaz, C. R.Kreller and N. J. Henson, *J. Electroanal. Chem.*, 2014, **720-721**, 34-40.
7 C. He, P. K. Shen, *Nano. Energy*, 2014, **8**, 52-61.
8 C. Tang, D. Wang, Z. Wu and B. Duan, *Int. J. Hydrogen Energ.,* 2015, **40**, 3229-3237.
9 Y. Oh, S. K. Kim, D. H. Peck, J. Jang, J. Kim and D. H. Jung, *Int. J. Hydrogen Energ.*, 2014, **39,** 15907-15912.
10 S. B. Yin, L. X. Yang, L. Luo, F. Huang, Y. H. Qiang, H. W. Zhang and Z. X. Yan, *New J. Chem.*, 2013, **37**, 3976-3980.
11 L. M. Jiang, H. G. Fu, L. Wang, W. Zhou, B. J. Jiang and R. H. Wang, *RSC Adv.,* 2014, **4**, 51272-51279.
12 Z. S. Li, S. Ji, B. G. Pollet and P. K. Shen, *Chem. Commun.,* 2014, **50**, 566-568.
13 N. R. Elezović, B. M. Babić, L. J. Gajić-Krstajić, P. Ercius, V. R. Radmilović, N. V. Krstajić, L. M. Vracar, *Electrochim. Acta,* 2012, **69**, 239-246.
14 C. He, H. Meng, X. Yao and P. K.Shen, *Int. J. Hydrogen Energ.*, 2012, **37**, 8154-8160.
15 I. J. Hsu, Y. C.Kimmel, Y. Dai, S. Chen, J. G. Chen, *J. Power Sources*, 2012, **199**, 46-52.
16 C. Liang, L. Ding, C. Li, M. Pang, D. Su, W. Li, Y. M. Wang, *Energ. Environ. Sci.*, 2010, **3**, 1121-1127.
17 V. Kiran, K. Srinivasu, S. Sampath, *Phys. Chem. Chem. Phys.,*2013, **15**, 8744-8751.
18 A. C. Garcia, E. A. Ticianelli, *Electrochim. Acta*, 2013, **106**, 453-459.

19 X. B. Gong, S. J. You, X. H. Wang, Y. Gan, R. N. Zhang, N. Q. Ren, *J. Power Sources*, 2013, **225,** 330-337.
20 C. K. Poh, S. H. Lim, Z. Tian, L. Lai, Y. P. Feng, Z. Shen, J. Y. Li, *Nano Energy*, 2013, **2**, 28-39.
21 P. Justin, P. H. K. Charan, G. R. Rao, *Appl. Catal. B*, 2014, **144**, 767-774.
22 Z. Yan, H. Meng, P. K. Shen, R. Wang, L. Wang, K. Shi and H. G. Fu, *J. Mater. Chem.*, 2012, **22**, 5072-5079.
23 Z. X. Yan, H. Wang, M. M. Zhang, Z. F. Jiang, T. Jiang, J. M. Xie, *Electrochim. Acta*, 2013, **95**, 218-224.
24 F. P. Hu, P. K. Shen. *J. Power Sources*, 2007, **173**, 877-881.
25 Y. Jin, D. Liu, X. Li and R. Yang, *Int. J. Refract. Met. H*, 2011, **29**, 372-375.
26 J. L. Lu, Z. H. Li, S. P. Jiang, P. K. Shen and L. Li, *J. Power Sources*, 2012, **202**, 56-62.
27 Z. Yan, F. Li, J. Xie and X. Miu, *RSC Adv*., 2015, **5**, 6790-6796.
28 L. Borchardt, M. Oschatz, S. Graetz, M. R. Lohe, M. H. Rümmeli and S. Kaskel, *Micropor. Mesopor. Mater.*, 2014, **186**, 163-167.
29 R. Wang, C. Tian, L. Wang, B. Wang, H. Zhang, H. Fu, *Chem. Commun.*, 2009, **21**, 3104-3106.
30 Z. Yan, M. Zhang, J. Xie, P. K. Shen, *J. Power. Sources*, 2013, **243**, 336-342.
31 Z. Q. Tian, S. P. Jiang, Y. M. Liang and P. K. Shen, *J. Phys. Chem. B*, 2006, **110**, 5343-5350.
32 J. D. Oxley, M. M. Mdleleni and K. S. Suslick, *Catal. Today*, 2004, **88,** 139-151.
33 J. C. Kim and B. K. Kim, *Scripta Mater.*, 2004, **50**, 969-972.
34 S. V. Pol, V. G. Pol and A. Gedanken, *Adv. Mater.,* 2006, **18**, 2023-2027.
35 S. Chouzier, P. Afanasiev, M. Vrinat, T. Cseri and M. Roy-Auberger, *Solid State Chem.,* 2006, **179**, 3314-3323.
36 Z. Yan, G. He, M. Cai, H. Meng, P. K. Shen, *J. Power Sources*, 2013, **242**, 817-823.
37 B. Lim, M. J. Jiang, P. H. C. Camargo, E. C. Cho, J. Tao, X. M. Lu, Y. M. Zhu and Y. N. Xia, *Science*, 2009, **324**, 1302-1305.
38 Z. Yan, G. He, P. K. Shen, Z. Luo, J. Xie and M. Chen, *J. Mater. Chem. A*, 2014, **2**, 4014-4022.
39 N. R. Elezovic, B. M. Babic, P. Ercius, V. R. Radmilovic, L. M. Vracar, N. V. Krstajic, *Appl. Catal. B,* 2012, **125**, 390-397.

Graphical abstract

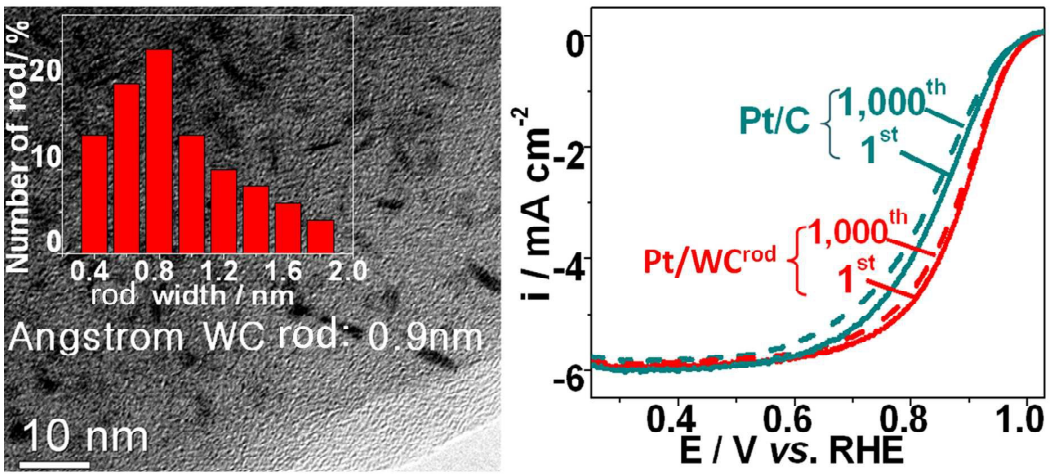

Pt/WC^{rod} shows higher ORR efficiency and stabilization than the commercial Pt/C